

Andrea L. Bertozzi · Jesus Rosado ·  
Martin B. Short · Li Wang

# Contagion shocks in one dimension

Received: date / Accepted: date

**Abstract** We consider an agent-based model of emotional contagion coupled with motion in one dimension that has recently been studied in the computer science community. The model involves movement with a speed proportional to a “fear” variable that undergoes a temporal consensus averaging based on distance to other agents. We study the effect of Riemann initial data for this problem, leading to shock dynamics that are studied both within the agent-based model as well as in a continuum limit. We examine the behavior of the model under distinguished limits as the characteristic contagion interaction distance and the interaction timescale both approach zero. The limiting behavior is related to a classical model for pressureless gas dynamics with “sticky” particles. In comparison, we observe a threshold for the interaction distance vs. interaction timescale that produce qualitatively different behavior for the system - in one case particle paths do not cross and there is a natural Eulerian limit involving nonlocal interactions and in the other case particle paths can cross and one may consider only a kinetic model in the continuum limit.

**Keywords** conservation laws · Riemann problem · contagion model · traffic flow

---

A. L. Bertozzi  
UCLA Department of Mathematics, Los Angeles, CA 90095  
E-mail: bertozzi@math.ucla.edu

J. Rosado  
UCLA Department of Mathematics, Los Angeles, CA 90095  
E-mail: jrosado@math.ucla.edu

M. B. Short  
Georgia Institute of Technology School of Mathematics, Atlanta, GA 30332  
E-mail: mbshort@math.gatech.edu

L. Wang  
UCLA Department of Mathematics, Los Angeles, CA 90095  
E-mail: liwang@math.ucla.edu

## 1 Introduction

A recent empirical analysis of computational emotional contagion models was studied in [41], in which various models were compared to video footage of crowd dynamics during an evacuation, to determine which of the models most accurately describe the behavior of the crowd. A model known as ASCRIBE [4], which we will study in detail in this paper, was observed to be the one most similar to the observed crowd dynamics. This model was subsequently used in an agent-based simulation tool (ESCAPES [42]) that incorporates emotional contagion in an evacuation scenario of the International Terminal at Los Angeles International Airport (LAX).

Though the ASCRIBE model reproduces actual crowd behavior well, running massive simulations of individual interacting agents can be computationally expensive and does not directly provide a theoretical understanding of the dynamic range and limits of the model. We present here an analysis of a contagion-movement model based on ASCRIBE, that provides insight into how the system behaves with very large numbers of particles, by taking a continuum limit of the agent-based model and examining what the ensuing issues are. This work has direct mathematical connection to related problems including traffic flow [3, 20, 24], swarming models [43, 12, 39, 40, 22], economics and social sciences [23, 16, 10], and pressureless gas models [6, 7, 25, 28, 31, 29, 44, 38, 27]. For simplicity, and to focus on a specific problem that captures some of the most interesting dynamics in one dimension, we focus on the Riemann problem and shock formation.

### 1.1 Discrete contagion models

The ASCRIBE model introduced in [4] involves moving, interacting agents, each of whom possesses an emotional variable  $q_i(t)$ , typically interpreted to represent fear or panic. The simplest form of the movement rule for these agents involves a speed proportional to the emotion level, so that the position  $x_i(t)$  of agent  $i$  evolves according to  $\dot{x}_i \propto q_i$ . The emotion  $q_i$ , meanwhile, undergoes a form of contagion, so that  $q_i$  equilibrates according to the consensus model

$$\dot{q}_i = \gamma(q_i^* - q_i), \quad q_i^* = \frac{\sum_{j \in G_i} w_{ij} q_j}{\sum_{j \in G_i} w_{ij}}. \quad (1)$$

Here,  $\gamma$  is an equilibration rate and  $G_i$  denotes the set of agents  $j$  that interacts with agent  $i$  with weights  $w_{ij}$ , so that  $q_i^*$  denotes a weighted average of emotion across this set. The weights could correspond to a straight average ( $w_{ij}$  constant) or depend on some environmental variable such as distance between agents. We note that the basic contagion model is a variant of a classical consensus model in control theory for which there is an extensive literature [21, 18, 13, 35].

The weights  $w$  in the full ASCRIBE model depend on five parameters for every pairwise interaction, based on the theory from [2]. These involve the level of sender's emotion  $q_j$ , level of receiver's emotion  $q_i$ , sender's expressiveness, receiver's openness, and the channel strength between the agents. The

study [41] compared it with another class of contagion model, the Durupinar model [17], which, in contrast to the previous one, uses a probabilistic threshold model based on epidemiological models of disease contagion [15, 30, 34, 37]. In [41], the authors identified key attributes of appropriate models using real data; namely, a video of an Amsterdam crowd scene [5] and a video of recent protests in Greece in which officers fired tear gas into a small crowd [14]. The ASCRIBE model produced a 14% improvement per agent per frame over the Durupinar model in a 15s clip and a 12% improvement in only a four-second clip.

As with consensus models, there is a strong connection between the contagion model and swarming models. In particular, when considered in one dimension, the emotion level  $q$  has the same role as the velocity in swarming models, and Equation (1) strongly reminds us of the Cucker-Smale formulation [12, 33]. In higher dimension, taking into account the emotion in addition to the position and velocity allows for a richer description of the behavior of gregarious groups [1].

## 1.2 Specific model studied in this paper

To focus on a problem that allows for mathematical analysis and insight into the general behavior of such models, we consider the following discrete Riemann problem and its continuum limits. Consider initial data consisting of an infinite number of agents spaced on the real line at grid points  $x_i = hi$  ( $i$  an integer), where  $h_L$  and  $h_R$  are the agent spacing to the left and right of zero, respectively. Assign  $q_i$  at time zero to be a value  $q_L$  for all  $i \leq 0$  and  $q_R$  for all  $i > 0$ , with all agents traveling to the right with a speed equal to their  $q$  value. The relevant dynamics occur when  $q_L > q_R$ , in other words, the agents with higher fear level try to push through the ones with a lower value. Each agent attempts to equilibrate his emotional level equally with any other agent within a distance  $R$  of himself. The dynamic equations for the emotion variable are then

$$\dot{q}_i = \gamma(q_i^* - q_i), \quad q_i^* = \frac{1}{N_i} \sum_{j, |x_j - x_i| < R} q_j, \quad \dot{x}_i = q_i, \quad (2)$$

where  $N_i$  is the number of  $j$ 's such that  $|x_j - x_i| < R$ , including  $i$ .

Although this is a simple model problem, it captures the kind of dynamics of interest, in which scared individuals are trying to push through others that are less scared in front of them. It also captures the basic contagion interactions from the ASCRIBE model with a fixed interaction radius. We can now study the behavior of this system as  $\gamma$  and  $R$  vary, and perform an analysis of the continuum limits in different settings. Later, we will also consider different interaction weights  $w_{ij}$ , and the interaction kernels that arise from them in the continuum limit.

### 1.3 Goals and organization

The remainder of this paper is organized as follows. Section 2 is dedicated to the microscopic description of the problem (2). We study in detail the conditions under which individual agents will maintain order, even if getting dangerously close to each other, or when this order will be broken. In Section 3, we consider the macroscopic limit. We start by considering the limiting case as the interaction radius  $R$  tends to zero and the equilibration rate  $\gamma$  tends to infinity in the particle setting and the corresponding singular shock formation in the macroscopic framework. Then we study the general case with finite equilibration rate and a more general interaction kernel. We again find conditions under which solutions will either remain bounded for all finite time or blow up in finite time. This framework is accurate while the characteristics of the equation do not intersect. When the characteristics do intersect, a kinetic approach is necessary; this is introduced in Section 4.

## 2 Microscopic description

In this section we want to study the qualitative behavior of a system of  $N$  agents whose dynamics is described by (1). First, we consider the case of only two interacting “particles” in the context of (2). Here, we use the term “particle” to refer to groups of  $n \geq 1$  agents that share the same position and velocity. In this setting, we can easily compute the exact solution and, specifically, determine whether the particle paths will cross, as is stated in the following Theorem:

**Theorem 1** *Let  $p_1$  and  $p_2$  be two particles located at positions  $x_1(0)$  and  $x_1(0) + d(0)$ , with velocities  $q_1(0)$  and  $q_2(0)$  and containing  $n_1$  and  $n_2$  agents, respectively, and  $d(0) \leq R$ . Then their paths will cross if and only if  $q_1(0) - q_2(0) > \gamma d(0)$ . Furthermore, if  $q_1(0) - q_2(0) > \gamma [d(0) + R]$ , their paths will cross and they will eventually cease to interact with each other. Furthermore, if the particles do cease interacting at some finite time, the speeds of the two particles after separation will be*

$$q_1 = q_1(0) - \frac{\gamma n_2 [d(0) + R]}{n_1 + n_2}, \quad q_2 = q_2(0) + \frac{\gamma n_1 [d(0) + R]}{n_1 + n_2}. \quad (3)$$

*Proof* Without loss of generality we can assume  $q_1(0) > q_2(0) \geq 0$ . With the particles  $p_1$  and  $p_2$  interacting only with each other, we have a conserved average fear level  $q^*$ :

$$q_1^* = q_2^* = q^* = \frac{n_1 q_1(0) + n_2 q_2(0)}{n_1 + n_2}. \quad (4)$$

In this situation, the emotion variables are given by:

$$q_1(t) = q^* + e^{-\gamma t} (q_1(0) - q^*); \quad (5)$$

$$q_2(t) = q^* + e^{-\gamma t} (q_2(0) - q^*). \quad (6)$$

We can then integrate these equations to find position information:

$$\begin{aligned} x_1(t) &= x_1(0) + \int_0^t q_1(s) ds \\ &= x_1(0) + q^*t + (1 - e^{-\gamma t})(q_1(0) - q^*)/\gamma, \\ x_2(t) &= x_1(0) + d(0) + \int_0^t q_2(s) ds \\ &= x_1(0) + d(0) + q^*t + (1 - e^{-\gamma t})(q_2(0) - q^*)/\gamma. \end{aligned}$$

Hence, the distance  $d(t) = x_2(t) - x_1(t)$  between the two particles is

$$d(t) = d(0) - \frac{q_1(0) - q_2(0)}{\gamma} (1 - e^{-\gamma t}) . \quad (7)$$

Given (7), we may first ask if the two particles will ever meet, i.e., is there any finite time at which  $d(t) = 0$ ? The answer is that the particles will meet only if

$$q_1(0) - q_2(0) > d(0)\gamma ; \quad (8)$$

that is, they will meet if the difference in speeds is sufficiently large relative to their initial separation and the equilibration rate. Similarly, we may ask if the two particles will ever stop interacting, i.e., is there any finite time at which  $d(t) < -R$ ? The answer is that the particles will stop interacting only if

$$q_1(0) - q_2(0) > [d(0) + R] \gamma . \quad (9)$$

Assuming that the particles stop interacting after a finite time  $t^*$ , that we can easily obtain from Equation (7), inserting  $t^*$  into Equations (5)-(6) will yield the last assertion of the statement.

Theorem 1 illustrates the relevance of the relation between the difference in the emotion level between two particles  $\Delta q$ , and the quantities  $\gamma\delta(0)$  and  $\gamma R$ . In the remainder of this section, let us discuss how this affects the behavior of the system when we consider more than two particles, in two different regimes.

## 2.1 Zero interaction radius, infinite equilibration rate

In a dense crowd setting, it is reasonable to assume a relatively small interaction radius and a rather quick equilibration rate. Thus, it is natural to consider the case in which  $R \rightarrow 0$ ,  $\gamma \rightarrow \infty$ . Let us further suppose, though, that as we approach these limiting values, the quantity  $R\gamma = C$  remains fixed, so that we can use the results of Theorem 1, with  $d(0) = R$  (since  $R \rightarrow 0$ , the particles will not interact until they are within distance  $R$  of each other for any non-zero initial spacing  $d(0)$ ) to determine if two particles may cross paths upon meeting. Specifically, Theorem 1 tells us that if the greatest difference in emotion between two particles  $\Delta q = q_L - q_R$  satisfies  $\Delta q \leq 2C$ , particle paths will never cross, while if  $\Delta q > 2C$ , particle paths may cross.

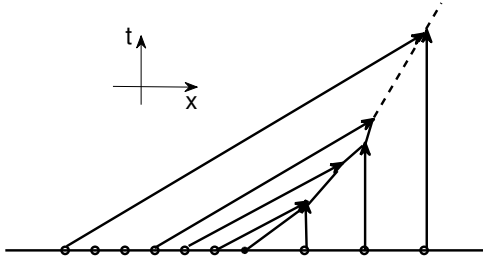


**Fig. 1** Description of particle characteristics with zero radius of interaction and infinite reaction time.

We first examine the case  $\Delta q \leq 2C$ ; here, agents do not interact until they collide, at which point they average their emotion/speed and stick together, which resembles the modeling of sticky particles in gas dynamics [6, 7, 25, 28, 44, 46]. In this case, we can solve the discrete Riemann problem exactly and the solution is a singular shock. Although this is unphysical – one would not expect individuals to simultaneously occupy the same position in space – it serves as a useful class of exact solutions to compare with the small  $R$  and large  $\gamma$  problems. We have the following theorem.

**Theorem 2** Consider the system (2) in which  $R = 0$  and agents average their fear and stick together when they collide. Then the solution satisfies

$$\begin{cases} x_i(t) = h_L i + q_L t & \text{for } i < (x_s(t) - q_L t)/h_L \\ x_i(t) = h_R i + q_R t & \text{for } i > (x_s(t) - q_R t)/h_R \\ x_i(t) = x_s(t) & \text{otherwise} \end{cases} \quad (10)$$

in which  $h_L$  (respectively  $h_R$ ) is the distance between two consecutive particles on the left side (respectively the right side) of the shock  $x_s(t)$ , which is the location of the accumulation of agents that collide from the left and from the right, satisfying  $\dot{x}_s(t) = \text{avg}_{i \in S}(q_i) := \frac{\sum_{i \in S} q_i}{\sum_{i \in S} 1}$ , where  $S$  is the set of all indices  $i$  such that the particle  $p_i$  belongs to the singular shock. Moreover, as  $t \rightarrow \infty$  we have  $\dot{x}_s \rightarrow s^*$  with

$$s^* = \frac{\sqrt{\rho_L} q_L + \sqrt{\rho_R} q_R}{\sqrt{\rho_R} + \sqrt{\rho_L}}, \quad (11)$$

where  $\rho_L = 1/h_L$  and  $\rho_R = 1/h_R$ , are the respective densities of agents on the left and the right.

The proof of this theorem can be found in the literature, such as [9] and the references therein, but we add it here for completeness.

*Proof* A diagram of the solution of the discrete problem is shown in Fig. 1, where one sees that the agents are independent of each other as long as they do not meet, but once they collide they stick together and form a shock. Therefore, the dynamics are well represented by (10). The asymptotic shock speed can be computed by noticing that the rate at which agents enter the shock from the left and from the right are respectively  $r_L = \rho_L(q_L - s^*)$  and  $r_R = \rho_R(s^* - q_R)$ . This gives an asymptotic shock speed of  $s^* = (r_L q_L + r_R q_R)/(r_L + r_R)$ . Combining these equations and solving the quadratic equation for  $s$  implies (11).

Now we consider the case when  $\Delta q > 2C$ , so that when two particles meet, they may pass through each other and then continue moving with separate trajectories. For simplicity's sake, let us consider here a symmetric initial state with respect to density, so that  $\rho_L = \rho_R = \rho_0$ . In this case, we switch into a frame of reference moving at the average speed  $s^* = (q_L + q_R)/2$ , which, due to symmetry, must be the shock speed. When the first two particles meet,  $p_0$  with speed  $q_L$  and  $p_1$  with speed  $q_R$ , they will certainly pass through each other, so that  $p_0$  will move ahead of the "shock" (that currently contains zero particles) while  $p_1$  will fall behind it. Once passed through the shock,  $p_0$  ( $p_1$ ) will have a reduced (increased) speed, as given in (3), and will continue to encounter particles of speed  $q_R < s^*$  ( $q_L > s^*$ ), causing further reductions (increases) in speed each time, and may even stick to some of the other particles encountered, given the reduced difference in speed relative to  $\Delta q$ . Hence,  $p_0$  ( $p_1$ ) will eventually reach a speed less than (greater than)  $s^*$ , and begin moving back toward the shock. When particles  $p_0$  and  $p_1$  (each now potentially a group of multiple agents) meet again, it will be at the location of the shock, due to symmetry, at which time they may pass through each other again, or may now stick together if the differences in their speeds is now less than  $2C$ . This same basic behavior is true of all the particles, so that the shock in this case will consist not only of a large particle moving at speed  $s^*$ , as it did in the sticky particle case above, but will also be surrounded by particles oscillating around the shock and passing through it, at least at small values of  $t$ .

The long-term behavior of the shock with regards to these oscillations can be determined by asking whether new particles entering the shock with speeds  $q_L$  or  $q_R$  are able to pass through any possible central shock particle moving at speed  $s^*$ . This will be the case if  $q_L - s^* > 2C$ , which is equivalent to  $\Delta q > 4C$ . Hence, in the case  $\Delta q > 4C$ , oscillations of particles around the shock will continue indefinitely, while in the case  $2C < \Delta q \leq 4C$ , the oscillations will quickly die out, and the long term behavior will be the same as that in the sticky particle case examined above, with a single massive particle moving at speed  $s^*$  serving as the shock. The indefinite oscillations case is illustrated in Fig. 2. The figure is constructed from a simulation that employs the analytic solution (3) for the case in which  $R \rightarrow 0$  and  $\gamma \rightarrow \infty$  with  $R\gamma = 1/30$  and  $d(0) = R$  (since we are considering the case  $R \rightarrow 0$ ), and exactly solves the resulting system as particles collide and potentially pass through each other.

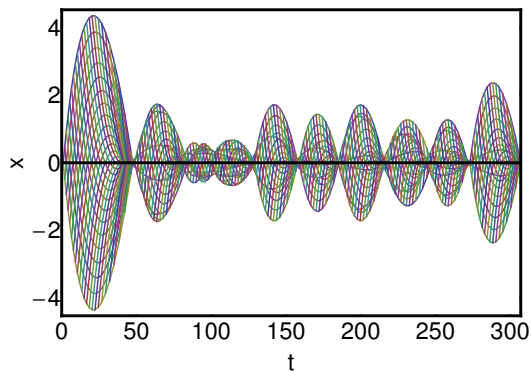


**Fig. 2** An example of the indefinite oscillations of particles passing through the central shock that occurs when  $\Delta q > 4C$ . Here,  $\Delta q = 1$  while  $C = 1/30$ , and the initial density of particles is 1. The colored lines correspond to the portions of the trajectories of particles after they have encountered at least one other particle or the central shock, as observed from a reference frame moving with the shock speed  $s^* = 1/2$ ; all other portions of trajectories are removed to allow for easier viewing of the oscillations.

## 2.2 Fast equalization

We now consider the model away from the limit  $R \rightarrow 0, \gamma \rightarrow \infty$ , that is, when the interaction radius is positive and the equilibration rate, albeit possibly large, is bounded, though still in the regime in which particle paths do not cross. As time advances, the framework we adopted for the previous discussion will not be valid: a positive radius of interaction will allow for multiple particles at different locations interacting at the same time, and possibly with different subsets of particles. Also, now it is possible for particles to equilibrate their levels of fear while still being at a positive distance from each other, leading us to consider an extended shock region with high accumulation of particles. A detailed description of the dynamics inside of the shock region, and in particular to be able to answer the question of whether or not the paths of any particles in it will eventually cross, requires a thorough analysis of the system of ODEs associated with the particles in the shock. This is not the goal of this paper, but a heuristic description of the behavior of this region will give us insight into the expected dynamics and provide a basis of comparison with the macroscopic formulation presented in the next section.

First, we adopt a framework where the initial distance between particles is larger than the interaction distance, so all interactions will occur around the shock region. As in Section 2.1, for the sake of simplicity we will assume symmetry with respect to the density in the following description. We start by considering the specific case when  $\Delta q = \gamma R$ ; in this case a sharp shock moving with velocity equal to the average initial velocities will form and, if the radius of interaction is small enough, the dynamics will resemble that of the sticky particle, as seen in Fig. 3.

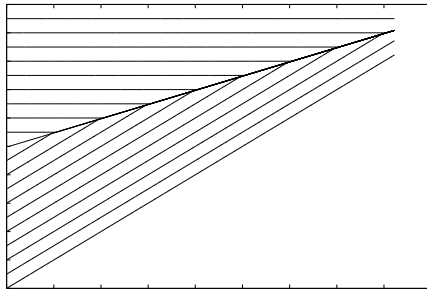


**Fig. 3** Shock Formation:  $q_L = 1$ ,  $q_R = 0$ ,  $\gamma = 200$ ,  $R = 0.005$ . Simulation done with 200 particles, set at an initial distance 1 from each other. Plot of 1 path every 10 particles.

What happens if  $\gamma$  and  $R$  do not satisfy this condition, though? If we vary  $\gamma$  and  $R$  in such a way that  $\Delta q < \gamma R$ , we are in the “swarming” regime where the contagion interaction happens fast compared to the length scale of the interactions. In this case, the particles emotion levels equilibrate before their paths can cross and the shock diffuses as the characteristics accumulate around the trajectory that would correspond with it, forming a sort of cone. This is seen in Fig. 4.

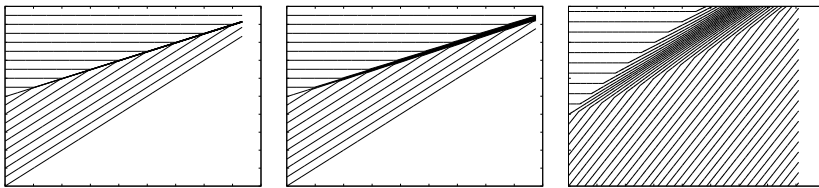


**Fig. 4** Diffusion of the shock. From left to right:  $N = 200$ ,  $q_L = 1$ ,  $q_R = 0$ ,  $\gamma = 10$ ,  $R = 0.1$ ;  $N = 200$ ,  $q_L = 1$ ,  $q_R = 0$ ,  $\gamma = 200$ ,  $R = 0.1$ ;  $N = 1000$ ,  $q_L = 1$ ,  $q_R = 0$ ,  $\gamma = 200$ ,  $R = 0.5$ . Particles set at an initial distance 1 from each other. Plot of 1 path every 10.

If, in addition, the interaction radius is large with respect to the starting distance between the particles, such that more particles interact simultaneously, the boundary of the cone loses its sharpness, and as the equilibration rate increases, velocities become uniform instantly (Fig. 5).

Moreover, in this regime, we must take into account that the effect of incoming particles will alter the relative distances among particles already in the shock region, which may potentially cross. As a consequence of this, the results summarized in Theorem 1 are not sharp any more. As we will see in the next section in detail, a macroscopic approach allows us to answer this question, and capture accurately the behavior we see in the microscopic description.

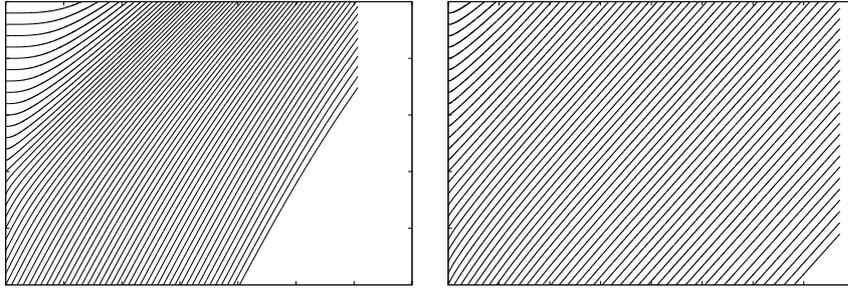


**Fig. 5** No sharp boundaries. From left to right:  $N = 1000$ ,  $q_L = 1$ ,  $q_R = 0$ ,  $\gamma = 10$ ,  $R = 5$ ;  $N = 1000$ ,  $q_L = 1$ ,  $q_R = 0$ ,  $\gamma = 200$ ,  $R = 5$ . Particles set at an initial distance 1 from each other. Plot of 1 path every 10.

Finally, if we vary  $\gamma$  and  $R$  in such a way that  $\Delta q > \gamma R$ , Theorem 1 tells us that particles will cross. As in the previous section, we are interested in the long time behavior of the shock, but again the fact that after crossing (maybe several times) particles can equilibrate at a positive distance from each other affects the asymptotic dynamics of the system. In this framework, we have to ask ourselves if a new incoming particle will escape *all* the particles already in the shock region (which may still be oscillating around the average speed  $s^*$ ). Instead of the sharp threshold observed in Section 2.1, now this will depend on the width of the shock region, not taking into account possible interaction-free islands inside it. Fig. 6 shows an example of the dynamics of the system in this framework.

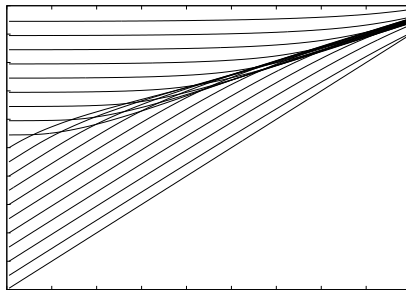


**Fig. 6** Crossing of characteristics ( $\Delta q > \gamma R$ ).  $q_L = 1$ ,  $q_R = 0$ ,  $\gamma = 0.5$ ,  $R = 0.1$ . Simulation done with 200 particles, set at an initial distance 1 of each other. Plot of 1 path every 10. Observe that, although  $4C = 4\gamma R = 0.2 \ll 1 = \Delta q$ , incoming particles do not oscillate indefinitely around the shock region but rather they are captured by it.

### 3 Macroscopic description

In this section, we study the dynamics of system (2) when the density of particles approaches infinity. When particle paths do not cross, we can directly obtain the macroscopic system without passing through the kinetic description. We first examine the macroscopic equivalent to the extreme case in Section 2.1. In this case, the continuum system is described by the pressureless Euler equations, while for the general interaction, studied next, we derive the macroscopic equations following the particle paths and show their correspondence with the particle model.

#### 3.1 Shock formation: zero interaction radius and infinite equilibration rate

The discrete solution proposed in Equation (10) in Section 2 has a continuum limit as described by a  $2 \times 2$  system of conservation law as follows

$$\rho_t + (Q)_x = 0; \quad Q_t + (Q^2/\rho)_x = 0, \quad (12)$$

where  $\rho$  is the local density of agents and  $Q$  is the local fear level weighted by the density of agents. As already mentioned in Section 2, this system arises as a model for sticky particles in gas dynamics. The solution admits a  $\delta$ -singularity, and has been analyzed extensively in the literature since 1994 [8, 6, 7, 11, 45, 25, 28, 31, 32, 36, 38, 29, 44, 27]. Below we present a derivation of the singular shock dynamics that will serve as a base model for the more general nonlocal problem.

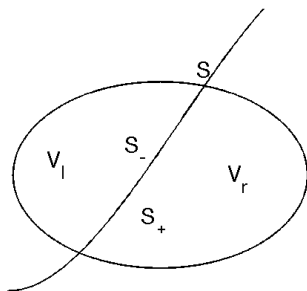


**Fig. 7** Open region  $V \subset \mathbb{R} \times [0, \infty)$  cut through by a curve  $S$  on which the singularity happens.

Define the local average fear level as  $q = Q/\rho$ ; from the microscopic dynamics, one sees that  $q$  is bounded from above and below, thus the singularity of system (12) only appears in  $\rho$  and  $Q$ , but not  $q$ . Therefore, the fluxes  $Q = \rho q$  and  $\frac{Q^2}{\rho} = \rho q^2$  are well defined in the distribution sense. Now, denote  $U = (\rho, Q)^T$ ,  $F(U) = (Q, Q^2/\rho)^T$ , and choose an open region

$V \subset \mathbb{R} \times [0, \infty)$  such that  $U$  is smooth on either side of a smooth curve  $S$ . We look for a measure solution that is classical on either side of  $S$  but may have mass accumulation as well as a jump discontinuity on  $S$ . This is a generalization of standard Rankine-Hugoniot theory [19]. Let  $V_l$  and  $V_r$  be the part on the left and right of the curve, respectively (see Fig. 7), and choose a smooth test function  $\varphi$  with compact support in  $V$ . Then a weak solution  $U$  satisfies

$$\begin{aligned}
0 &= \int_V U \varphi_t + F(U) \varphi_x dx dt \\
&= \int_{V_l} U \varphi_t + F(U) \varphi_x dx dt + \int_{V_r} U \varphi_t + F(U) \varphi_x dx dt + \int_{S^-}^{S^+} U \varphi_t + F(U) \varphi_x dx dt \\
&= - \int_{V_l} (U_t + F_x) \varphi dx dt + \int_{S^-} (U^- \nu_1 + F^- \nu_2) \varphi d\Gamma - \int_{V_r} (U_t + F_x) \varphi dx dt \\
&\quad - \int_{S^+} (U^+ \nu_1 + F^+ \nu_2) \varphi d\Gamma + \int_{S^-}^{S^+} U \left( \varphi_t + \frac{dx_S(t)}{dt} \varphi_x \right) dx dt \\
&= \int_{t_1}^{t_2} \left( \frac{dx_S}{dt} [U] - [F(U)] \right) \varphi dt + \int_{t_1}^{t_2} M(t) \frac{d\varphi(x_S(t), t)}{dt} dt \\
&= \int_{t_1}^{t_2} \left( \frac{dx_S}{dt} [U] - [F(U)] - \frac{dM(t)}{dt} \right) \varphi dt, \tag{13}
\end{aligned}$$

where we use the fact that along the curve  $S$ , the flux satisfies  $F(u(x_S(t), t)) = \frac{dx_S(t)}{dt} u(x_S(t), t)$  by definition. Here  $M = \int_{S^-}^{S^+} U dx dt = \int_{t_1}^{t_2} dt \int_{x_S(t)^-}^{x_S(t)^+} U dx$  is the singular mass. Therefore, we have

$$\frac{dM_\rho(t)}{dt} = s^* [\rho] - [Q], \quad \frac{dM_Q(t)}{dt} = s^* [Q] - [Q^2/\rho], \tag{14}$$

where  $s^*(t) = \frac{dx_S(t)}{dt}$ .

However, relation (14) is not enough to uniquely define the weak solution for (12) with Riemann initial data, since  $s^*$  is unknown. Sheng and Zhang in [38] derive this speed by constructing a delta distribution solution as a vanishing viscosity solution of (12) with a Dafermos regularization. Cheng et. al revisit it in [11] in the vanishing pressure framework. Here we derive the shock speed in a very simple way. Notice that the singular mass  $M_\rho(t)$  describes the total number of agents accumulated along  $S$ ,  $M_Q(t)$  describes the total amount of fear along  $S$ , and the shock speed  $s^*$  represents the average fear level. Thus we have the constitutive relation

$$M_Q(t) = s^* M_\rho(t). \tag{15}$$

Combining it with (14) immediately leads to (11). This derivation indeed shares the same spirit as the derivation of Theorem 2 for the agent based model.

### 3.2 Fast equalization with nonlocal spatial interactions

In this subsection, we consider the dynamics in Section 2.2 in the limit as the particle density goes to infinity. We work in the regime where particles will adjust their speed to that of their neighbors quickly enough so as to not cross each other, thus we can derive the limit in a Lagrange formulation. Consider the flow map  $X(\alpha, t)$  such that

$$\frac{dX(\alpha, t)}{dt} = q(X(\alpha, t), t), \quad X(\alpha, 0) = \alpha. \quad (16)$$

Then the changing of fear level  $q$  can be written as  $\frac{Dq}{Dt} = \gamma(q^* - q)$ , which, going back to the Eulerian variable, reads  $q_t + qq_x = \gamma(q^* - q)$ . Combining this equation with the conservation of mass, we have a macroscopic model as follows:

$$\rho_t + (\rho q)_x = 0, \quad (17)$$

$$q_t + qq_x = \gamma(q^* - q), \quad q^* = \frac{K * (\rho q)}{K * \rho}, \quad (18)$$

with Riemann initial data

$$\rho(x, 0) = \rho_0, \quad q(x, 0) = \begin{cases} q_L, & x < 0, \\ q_R, & x > 0, \end{cases}, \quad q_L > q_R. \quad (19)$$

We will specify the interaction kernel  $K$  later. Compared to (12), this model takes into account the positive radius of interaction and finite reaction time.

As mentioned in Section 3.1, for zero radius of interaction and infinite equilibration rate, a singular shock will happen in the macroscopic model corresponding to the mass concentration in the particle model. Then for (17)–(18), will we still see mass concentration? That is, will  $\rho$  stay uniformly bounded for any time  $T$  or blow up in finite time? First we have the following results.

**Theorem 3** *Consider the system (17)–(18) with initial data  $\rho(x, 0) = \rho_0$ ,  $\partial_x q(x, 0) \leq 0$  and  $\lim_{x \rightarrow -\infty} q(x, 0) = q_L$ ,  $\lim_{x \rightarrow \infty} q(x, 0) = q_R < q_L$ . Then, if  $\max_x |\partial_x q(x, 0)| > \gamma$ ,  $\rho$  will blow up in finite time.*

*Proof* Let  $\omega = -q_x$ ,  $\omega^* = -(q^*)_x$  and take the derivative in  $x$  of (18), we have

$$\omega_t + q\omega_x = \omega^2 + \gamma\omega^* - \gamma\omega. \quad (20)$$

Now, consider the flow map  $X(\alpha, t)$  such that

$$\frac{dX(\alpha, t)}{dt} = q(X(\alpha, t), t), \quad X(\alpha, 0) = \alpha.$$

Then (17) and (20) become

$$\frac{D\rho}{Dt} = \rho\omega(X(\alpha, t), t), \quad \frac{D\omega}{Dt} = \omega^2 + \gamma\omega^* - \gamma\omega. \quad (21)$$

Therefore, if  $\max_x |\partial_x q(x, 0)| = |\omega(X(\alpha_c, 0), 0)| > \gamma$ ,  $\frac{D\omega}{Dt} > 0$ , and thus  $\omega(x, t)$  is growing with time, whence  $\omega^2 - \gamma\omega + \gamma\omega^* > 0$  for any  $T$  by noticing that  $\omega^*$  stays nonnegative. Moreover, from (21) one sees that  $\frac{D\omega}{Dt} > \omega^2 - \gamma\omega$ , which implies  $\omega(X(\alpha_c, t), t) > \frac{\gamma}{1 - (1 - \frac{\gamma}{\omega(X(\alpha_c, 0), 0)})e^t}$  and leads to finite time blow up.

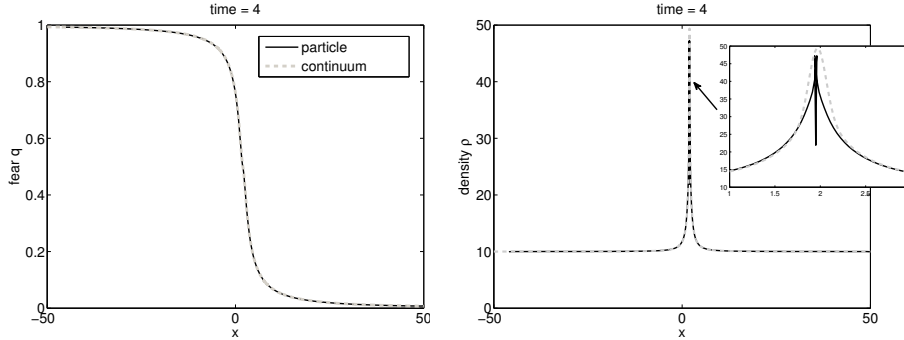


**Fig. 8** Comparison of simulation of macroscopic model (17)–(18), (22) with  $\rho_0 = 10$ ,  $q_L = 1$ ,  $q_R = 0$  and and particle model (23) with the same initial data for  $q$  and 1000 particles in domain  $[-50, 50]$  at time  $t = 4$ . Here  $\gamma = 5$ ,  $R = 0.1$ .

To illustrate this behavior, we choose a smoothed Riemann initial data  $q(x, 0) = (1 - \tanh(20x))/2$ , so that  $q_L = 1$  and  $q_R = 0$ , and let  $\rho_0 = 10$ ,  $R = 0.1$ , and  $\gamma = 5$ . The kernel takes the form

$$K(x) = \frac{1}{x^2 + R^2} \frac{R}{\pi}. \quad (22)$$

From the above theorem, we expect the crossing of characteristics in this case. To see this, we solve (17)–(18) numerically and compare it with the particle model

$$\dot{q}_i = \gamma(q_i^* - q_i), \quad q_i^* = \frac{\sum_{j=1}^N K(|x_j - x_i|)q_j}{\sum_{j=1}^N K(|x_j - x_i|)}, \quad \dot{x}_i = q_i \quad (23)$$

using the same initial data for  $q$  and 1000 particles uniformly distributed in the domain  $[-50, 50]$ . The plots of density  $\rho$  and fear  $q$  at time = 4 are displayed in Fig. 8, where the density plot clearly implies the crossing. Though particles have crossed at this time, the plot of  $q(x, 4)$  still matches very well between the particle and continuum versions at the scales illustrated here. This is because the values of  $\gamma$  and  $R$  we chose here are right near the edge for blowing up and particles equilibrate very quickly after crossing. If we decrease  $\gamma$ , we will more clearly see a multivalued solution for  $q$  in the particle case, resulting in a discrepancy of the two models; we will see this in more detail in Section 4. It is also interesting to point out that even in the presence of particles crossing, the macroscopic model still captures the correct shock speed.

**Theorem 4** For the system (17)–(18) with initial data  $\rho(x, 0) = \rho_0$ ,  $\partial_x q(x, 0) \leq 0$ ,  $\lim_{x \rightarrow -\infty} q(x, 0) = q_L$ ,  $\lim_{x \rightarrow \infty} q(x, 0) = q_R < q_L$ , assume that there exist a constant  $C_1$  such that the kernel satisfies  $K'(x) \leq C_1 K(x)$ , then if  $\max_x |\partial_x q(x, 0)| \leq \frac{\gamma}{2}$ ,  $\gamma > 8C_1 q_L$ , then for any time  $T$ , we have  $\rho < C_2 T$  with  $C_2$  being a constant.

In order to prove Theorem 4, we need the result in the following lemma, regarding the uniform boundedness of  $\omega^*$ .

**Lemma 1** If the Kernel  $K \in W^{2,1}$  and there is a constant  $C_1$  such that  $K$  satisfies  $|K'(x)| \leq C_1 K(x)$ , then  $\omega^*$  is uniformly bounded.

*Proof* From the definition of  $\omega^*$ , we have

$$\begin{aligned} |\omega^*| &= \left| \frac{(K * \rho_x)(K * \rho q) - (K * (\rho q))_x (K * \rho)}{(K * \rho)^2} \right| \\ &= \left| \frac{(K_x * \rho)(K * \rho q) - (K_x * (\rho q))(K * \rho)}{(K * \rho)^2} \right|, \end{aligned}$$

where we have used integration by parts since  $K \in W^{2,1}$ . Notice that since  $q < \max\{q_L, q_R\}$ , we have

$$|\omega^*| \leq 2 \max\{q_L, q_R\} \left| \frac{K_x * \rho}{K * \rho} \right| \leq 2C_1 \max\{q_L, q_R\} \quad (24)$$

*Proof (Proof of Theorem 4)* As in the proof of Theorem 3, we look at equation (21) for  $\omega^*$ . Since  $4\omega^* \ll 8C_1 q_L < \gamma$ , the polynomial  $\omega^2 - \gamma\omega + \gamma\omega^*$  always has two real roots  $R_{1/2}(\omega^*) = \frac{1}{2} \left( \gamma \pm \sqrt{\gamma^2 - 4\gamma\omega^*} \right)$ , and  $0 \leq R_1(\omega^*) \leq \frac{\gamma}{2} \leq R_2(\omega^*) \leq \gamma$ . Therefore, if initially  $R_1(\omega(\alpha, 0)) < \omega(\alpha, 0) < \frac{\gamma}{2}$ , we will have  $\frac{D\omega}{Dt} < 0$ . In the same way, if initially  $\omega(\alpha, 0) < R_1(\omega(\alpha, 0), 0)$ ,  $\frac{D\omega}{Dt} > 0$  and  $\omega$  increases, but once it surpasses the value of  $R_1(\omega)$  it decreases again. So in both cases  $\omega$  will never increase over  $\frac{\gamma}{2}$ . Then from the expression for  $\rho$

$$\rho(X(\alpha, t), t) = \rho(X(\alpha, 0), 0) e^{\int_0^t \omega(X(\alpha, \tau), \tau) d\tau}, \quad (25)$$

we see that for any  $T > 0$ ,  $\max_\alpha \rho(\alpha, t) < \max_\alpha \rho(\alpha, 0) e^{\frac{\gamma}{2} T}$ .

We also compare the solutions of both particle and macroscopic models under the assumptions of Theorem 4 in Fig. 9. Here  $\rho$  remains bounded and good agreements are observed. In fact, for the case in Theorem 4, we see that  $\omega$  is not only uniformly bounded, but also decaying to zero with time, as illustrated in Fig. 10, which gives a profile of  $\omega(X(0, t), t)$  versus  $t$ . As one can see, the decay rate of  $\omega(X(0, t), t)$  is approximately  $1/t$ , so  $\rho$  will have infinite time blow up.

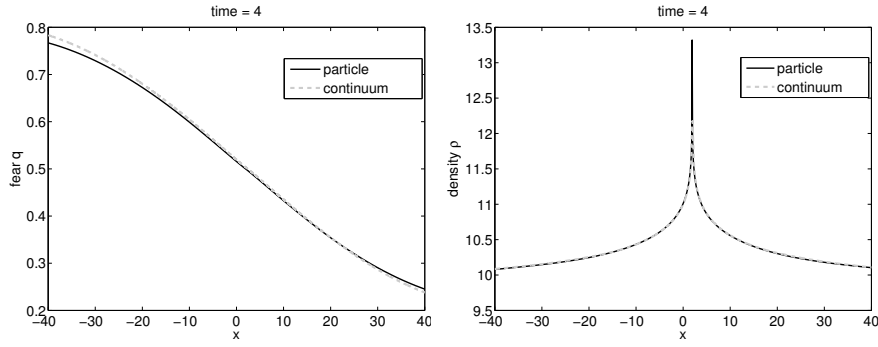


**Fig. 9** Comparison of a simulation of macroscopic model (17)–(18), (22) with  $\rho_0 = 10$ ,  $q_L = 1$ ,  $q_R = 0$  and particle model (23) with the same initial data for  $q$  and 1000 particles in domain  $[-50,50]$  at time  $t = 4$ . Here  $\gamma = 110$ ,  $R = 0.1$ .

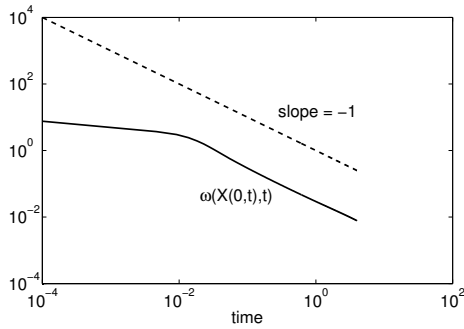


**Fig. 10** Plot of  $\omega(X(0,t), t)$  versus time in log scale for macroscopic model (17)–(18), (22) with  $\rho_0 = 10$ ,  $q_L = 1$ ,  $q_R = 0$ ,  $\gamma = 110$ ,  $R = 0.1$ .

#### 4 Crossing characteristics: kinetic description

For parameters and initial conditions that lead to particle crossing, the PDE description of (12) will fail to replicate the behavior of the particles after the crossing time, which corresponds to the blow-up of the PDEs as discussed in Theorem 3. However, following classical results from kinetic theory, we could use the BBGKY hierarchy to describe the evolution of the particle system with a single PDE in multiple dimensions. That is, we can consider the  $N$ -particle distribution in the space/emotion phase space

$$F^N(x_1, q_1, \dots, x_N, q_N, t), \quad (x_i, q_i) \in \mathbb{R} \times [0, 1] \quad i = 1, \dots, N$$

and the corresponding Liouville equation. Under the assumption of symmetry and indistinguishability of the particles, the system can be described by the marginal associated to one of the particles, say, the first one:

$$f := f_1^N(t, x, q) := \int_{R^{2(N-1)}} F^N(x_1, q_1, \dots, x_N, q_N, t) dx_2 \dots dx_N dq_2 \dots dq_N$$

Integrating the Liouville equation will yield

$$\frac{\partial f}{\partial t} + q \frac{\partial f_1^N}{\partial x} = \text{Interaction Term},$$

where the term on the right hand side of the equation depends on the partial derivatives with respect to  $q$  of  $f_1^N$  and the second marginal

$$f_2^N(t, x_1, x_2, q_1, q_2) := \int_{\mathbb{R}^{2(N-2)}} F_N dx_3 \dots dx_N dq_3 \dots dq_N.$$

The evolution of  $f_2^N$  would depend on  $f_3^N$ , which in turn depends on  $f_4^N$  and so on. Nevertheless, in the thermodynamic limit of very large numbers of agents, the chaos assumption holds, and thus we can approximate  $f_2^N(t, x_1, x_2, q_1, q_2) \sim f_1^N(t, x_1, q_1) f_1^N(t, x_2, q_2)$  thus the force term can be simplified, yielding the kinetic equation

$$\frac{\partial f(t, x, q)}{\partial t} + q \frac{\partial f(t, x, q)}{\partial x} = \frac{\partial}{\partial q} [\gamma (q - q^*(x, t)) f(t, x, q)]. \quad (26)$$

Here,  $f(t, x, q)$  is the density of agents with fear  $q$  at the point  $x$  at time  $t$ , and  $q^*(x, t)$ , the average fear at location  $x$  at time  $t$ , would be given by

$$\bar{q}(x, t) = \frac{\int \int q' f(t, x', q') K(x, x') dq' dx'}{\int \int f(t, x', q') K(x, x') dq' dx'}, \quad (27)$$

where  $K(x, x')$  is the interaction kernel between the particles at location  $x$  and  $x'$ . It should be noted that this equation is only a valid approximation of a particle system of infinite density, as was also the case of the PDE model in (12). A detailed derivation for the similar Cucker-Smale equation for swarming can be found in [26, ?], and for the general  $N$ -dimensional case of the contagion model in [1].

Simulations of (26) are compared to the results of the agent-based system and the PDEs (12) in Fig. 11. Here, we use  $\gamma = 0.1$ ,  $K(x, x') = [1 + (x - x')^2/R^2]^{-1}$ ,  $R = 0.1$ , a spatial domain of length  $L = 160$  with 1600 particles, and initial fear distribution

$$q(x, 0) = 0.5 [1 + \tanh(0.25(80 - x))] , \quad (28)$$

which will lead to eventual particle path crossing. There is general agreement between the particle and kinetic simulations, though the numerical method used to solve the kinetic equation contains non-negligible numerical diffusion, causing the kinetic solutions to be smoothed out relative to the agent-based simulation. The PDE model, however, does not describe the particles well at this point in time, as it insists upon a sharp shock that particles cannot cross through, while the particles and kinetic equation allow the passage of individuals through the shock, causing it to be much more spatially extended than the PDE will allow.

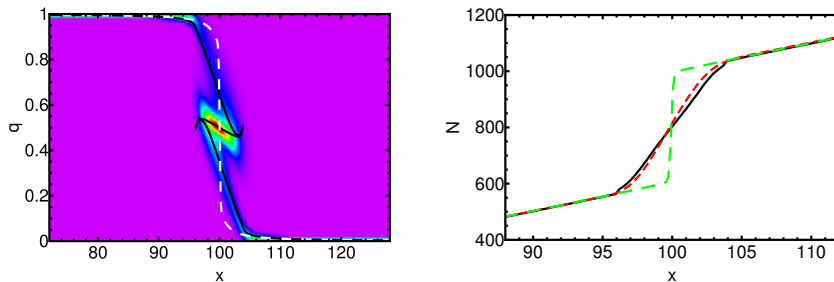


**Fig. 11** Comparing results of the particle, kinetic, and PDE models after particle crossing has occurred, using parameters and initial conditions described in the text. (Left) Colorplot of the kinetic distribution  $f(40, x, q)$ , with colors ranging from purple at low values to red at high values. Overlaid on the colorplot are the  $q(x, 40)$  values obtained from both the particle model (solid, black) and the PDE model (dashed, white). Both the kinetic and particle models display a wide shock due to agents passing through each other, while the PDE results show a very narrow shock. (Right) Plots of the cumulative density distribution  $N(x)$  (number of agents with position  $y \leq x$ ) at time  $t = 40$  obtained for particles (solid, black), the kinetic equation (red, short-dashed), and the PDE system (green, long-dashed). The kinetic and particle models match well even over the shock region, while the PDE model does not.

## 5 Summary and Conclusions

In this work, we considered a system of interacting agents that move in one dimension according to the intensity of some emotion that spreads and equilibrates through the agents, and studied the dynamics of this system at three different levels: microscopic, macroscopic, and kinetic.

We provide a thorough description of the behavior of the system at the microscopic level in terms of the relation between the difference in emotion intensity between two consecutive agents  $\Delta q$  and the quantity  $C = \gamma R$  that characterizes how fast agents equilibrate in relation to the characteristic length at which the interaction happens. In the regime where  $\gamma \rightarrow \infty$  and  $R \rightarrow 0$  we observe three different regimes: for  $\Delta q < 2C$  we recover the classical sticky particle model; for  $2C < \Delta q < 4C$  particles will initially cross but eventually converge on the trajectory of the shock such that new incoming particles will not cross the shock but adhere to it; and for  $\Delta q > 4C$  particles oscillate indefinitely through the shock. For finite  $\gamma$  and strictly positive  $R$ , we observe that if particles do not cross, as we move away from the limit the shock becomes smoother, and we talk about a shock region with high density of particles that grows with time. If particles do cross, a shock region will also form but in this case the effect of a large  $\Delta q$  will be an increase in the width of this region, that eventually will capture any newly approaching particle.

At the macroscopic level, we first recover the continuum version of the sticky particle model and provide a formula for the asymptotic speed of the shock. Then we use the Eulerian formulation to derive a continuum equation with the same dynamics as the particle system when the equilibration rate is finite and the characteristic interaction length is strictly positive. In this

framework we consider more general kernels than the one introduced in the microscopic description, and we can provide a theory for when the solution will blow up, corresponding to crossing of characteristics (or particles in the microscopic formulation). Namely, we see that if  $|\partial_x q(x, 0)| > \gamma$  then the density  $\rho$  will blow up in finite time, while if  $\max_x |\partial_x q(x, 0)| \leq \frac{\gamma}{2}$ ,  $\gamma > 8C_1 q_L$ , and for certain classes of kernels, then  $\rho$  will remain bounded. The blow up of the density is of particular interest, since it corresponds in the model to areas of high risk within a crowd where individuals can be trampled on by their neighbors. Understanding the behavior of the system in the regime  $\frac{\gamma}{2} < |\partial_x q| < \gamma$  is still an open question.

Finally, we formally derive a kinetic equation that provides a continuous description of the particle model when the characteristics of the PDE cross, so that the PDE model does not capture the dynamics of the particle system accurately. We show a numerical example of how, with the kinetic description, we can again recover the behavior observed at the microscopic level.

## Acknowledgments

The authors want to thank Millind Tambe and Jason Tsai for setting us on the tracks to the problem that motivated this work and all the discussions that followed. This work has been supported by ARO MURI grant W911NF-11-1-0332, NSF grant DMS-0968309, NSF grant DMS-0907931, and ARO grant W911NF1010472.

## References

1. A. Barbaro and J. Rosado. Contagion models for crowd behavior in panic situations. Preprint.
2. S.G. Barsade and D.E. Gibson. Group emotion: A view from top and bottom. In D. Gruenfeld, E. Mannix, and M. Neale, editors, *Research on Managing on Groups and Teams*, pages 81–102, Stamford, 1998. JAI Press.
3. N. Bellomo, M. Delitala, and V. Coscia. On the mathematical theory of vehicular traffic flow. I. Fluid dynamic and kinetic modelling. *Math. Models Methods Appl. Sci.*, 12(12):1801–1843, 2002.
4. T. Bosse, R. Duell, Z.A. Memon, J. Treur, and C.N.V.D. Wal. A multi-agent model for mutual absorption of emotions. In *European Council on Modeling and Simulation, ECMS 2009*, pages 212–218, 2009.
5. T. Bosse, M. Hoogendoorn, M. Klein, J. Treur, and N. van der Wal. Agent-based analysis of patterns in crowd behaviour involving contagion of mental states. In *IEA/AIE 2011*, Heidelberg, 2011. Springer.
6. F. Bouchut. On zero pressure gas dynamics. In *Advances in kinetic theory and computing*, volume 22 of *Ser. Adv. Math. Appl. Sci.*, pages 171–190. World Sci. Publ., River Edge, NJ, 1994.
7. François Bouchut and François James. Duality solutions for pressureless gases, monotone scalar conservation laws, and uniqueness. *Comm. Partial Differential Equations*, 24(11-12):2173–2189, 1999.
8. François Bouchut, Shi Jin, and Xiantao Li. Numerical approximations of pressureless and isothermal gas dynamics. *SIAM Journal on Numerical Analysis*, 41(1):pp. 135–158, 2004.
9. Yann Brenier and Emmanuel Grenier. Sticky particles and scalar conservation laws. *SIAM J. NUMER. ANAL.*, pages 2317–2328, 1998.

10. A. Chakraborti. Distributions of money in models of market economy. *Int. J. Modern Phys. C*, 13:1315–1321, 2002.
11. Gui-Qiang Chen and Hailiang Liu. Formation of  $\delta$ -shocks and vacuum states in the vanishing pressure limit of solutions to the Euler equations for isentropic fluids. *SIAM J. Math. Anal.*, 34(4):925–938, 2003.
12. F. Cucker and S. Smale. Emergent behavior in flocks. *IEEE Trans. Automat. Control*, 52:852–862, 2007.
13. P. Degond, J. G. Liu, and C. Ringhofer. Large-scale dynamics of mean-field games driven by local nash equilibria. to appear in: *Journal of Nonlinear Science*.
14. J. Diamond, M. McVay, and M.W. Zavala. Quick, safe, secure: Addressing human behavior during evacuations at lax, 2010. Master’s thesis, UCLA Dept of Public Policy.
15. P. Dodds and D.J. Watts. A generalized model of social and biological contagion. *Journal of Theoretical Biology*, 232(4):587–604, 2005.
16. A. Dragulescu and V. M. Yakovenko. Statistical mechanics of money. *Eur. Phys. Jour. B*, 17:723–729, 2000.
17. F. Durupinar. *From Audiences to Mobs: Crowd Simulation with Psychological Factors*. PhD thesis, Bilkent University, Dept. Comp. Eng., 2010.
18. B. Dring. Kinetic modelling of opinion leadership. *SIAM News*, 44(10):1–8, 2011.
19. L. Evans. *Partial differential equations*. 2010.
20. S. Fan and B. Seibold. A comparison of data-fitted first order traffic models and their second order generalizations via trajectory and sensor data. In *Proceedings of the Transportation Research Board, 92nd Meeting*, 2013.
21. E. Ferrante, A. E. Turgut, C. Huepe, A. Stranieri, C. Pinciroli, and M. Dorigo. Self-organized flocking with a mobile robot swarm: a novel motion control method. *Complete data*, 2012.
22. R. C. Fetecau, Y. Huang, and T. Kolokolnikov. Swarm dynamics and equilibria for a nonlocal aggregation model. *Nonlinearity*, 24(10):2681–2716, 2011.
23. S. Galam, Y. Gefen, and Y. Shapir. Sociophysics: a new approach of sociological collective behavior. *J. Math. Sociology*, 9:1–13, 1982.
24. I. Gasser. On non-entropy solutions of scalar conservation laws for traffic flow. *Zeitschr. f. Angew. Math. Mech. ZAMM*, 83(2):137–143, 2003.
25. Emmanuel Grenier. Existence globale pour le système des gaz sans pression. *C. R. Acad. Sci. Paris Sér. I Math.*, 321(2):171–174, 1995.
26. S. Y. Ha and E. Tadmor. From particle to kinetic and hydrodynamic descriptions of flocking. *Kinetic and Related Models*, 1:415–435, 2008.
27. F. Huang and Z. Wang. Well posedness for pressureless flow. *Commun. Math. Phys.*, 222:117–146, 2001.
28. Feimin Huang and Zhen Wang. Well posedness for pressureless flow. *Comm. Math. Phys.*, 222(1):117–146, 2001.
29. Feimin Huang and Zhen Wang. Well posedness for pressureless flow. *Comm. Math. Phys.*, 222(1):117–146, 2001.
30. W.O. Kermack and A.G. McKendrick. A contribution to the mathematical theory of epidemics. *Proceedings of The Royal Society of London. Series A*, 115:700–721, 1927.
31. Jiequan Li and Hanchun Yang. Delta-shocks as limits of vanishing viscosity for multidimensional zero-pressure gas dynamics. *Quart. Appl. Math.*, 59(2):315–342, 2001.
32. Jiequan Li and Tong Zhang. Generalized Rankine-Hugoniot relations of delta-shocks in solutions of transportation equations. In *Advances in nonlinear partial differential equations and related areas (Beijing, 1997)*, pages 219–232. World Sci. Publ., River Edge, NJ, 1998.
33. S. Motsch and E. Tadmor. A new model for self-organized dynamics and its flocking behavior. *Journal of Statistical Physics, Springer*, 144(5):923–947, 2011.
34. J.D. Murray. *Mathematical Biology*. Springer, New York, 2002.
35. L. Perea, G. Gómez, and P. Elosegui. Extension of the cucker-smale control law to space flight formations. *AIAA Journal of Guidance, Control, and Dynamics*, 32:527–537, 2009.

- 
36. F. Poupaud and M. Rascle. Measure solutions to the linear multi-dimensional transport equation with non-smooth coefficients. *Comm. Partial Differential Equations*, 22(1-2):337–358, 1997.
  37. T.C. Schelling. Hockey helmets, concealed weapons, and daylight saving: a study of binary choices with externalities. *Journal of Conflict Resolution*, 17:381–428, 1973.
  38. Wancheng Sheng and Tong Zhang. The Riemann problem for the transportation equations in gas dynamics. *Mem. Amer. Math. Soc.*, 137(654):viii+77, 1999.
  39. C. M. Topaz and A. L. Bertozzi. Swarming patterns in a two-dimensional kinematic model for biological groups. *SIAM J. Appl. Math.*, 65:152–174, 2004.
  40. C. M. Topaz, A. L. Bertozzi, and M. A. Lewis. A nonlocal continuum model for biological aggregation. *Bulletin of Mathematical Biology*, 68(7):1601–1623, 2006.
  41. Jason Tsai, Emma Bowring, Stacy Marsella, and Milind Tambe. Empirical evaluation of computational emotional contagion models. In *Proceedings of the 10th international conference on Intelligent virtual agents, IVA'11*, pages 384–397, Berlin, Heidelberg, 2011. Springer-Verlag.
  42. Jason Tsai, Natalie Fridman, Emma Bowring, Matthew Brown, Shira Epstein, Gal Kaminka, Stacy Marsella, Andrew Ogden, Inbal Rika, Ankur Sheel, Matthew E. Taylor, Xuezhi Wang, Avishay Zilka, and Milind Tambe. Escapes: evacuation simulation with children, authorities, parents, emotions, and social comparison. In *The 10th International Conference on Autonomous Agents and Multiagent Systems - Volume 2, AAMAS '11*, pages 457–464, Richland, SC, 2011. International Foundation for Autonomous Agents and Multiagent Systems.
  43. T. Vicsek, A. Cziròk, E. Ben-Jacob, I. Cohen, and O. Shochet. Novel type of phase transition in a system of self-driven particles. *Phys. Rev. Lett.*, 75:1226–1229, 1995.
  44. Zhen Wang, Feimin Huang, and Xiaqi Ding. On the Cauchy problem of transportation equations. *Acta Math. Appl. Sinica (English Ser.)*, 13(2):113–122, 1997.
  45. E. Weinan, Yu. G. Rykov, and Ya. G. Sinai. Generalized variational principles, global weak solutions and behavior with random initial data for systems of conservation laws arising in adhesion particle dynamics. *Comm. Math. Phys.*, 177(2):349–380, 1996.
  46. W. E. Yu, G. Rykov, and Ya. G. Sinai. Generalized variational principles, global weak solutions and behavior with random initial data for systems of conservation laws arising in adhesion particle dynamics. *Commun. Math. Phys.*, 177:349–380, 1996.